Stene, Riane E.; Scheibe, Benjamin; Pietzonka, Clemens; Karttunen, Antti J.; Petry, Winfried; Kraus, Florian

MoF_5 revisited. A comprehensive study of MoF_5

Published in:
Journal of Fluorine Chemistry

DOI:
10.1016/j.jfluchem.2018.05.002

Published: 01/07/2018

Document Version
Peer-reviewed accepted author manuscript, also known as Final accepted manuscript or Post-print

MoF_5 revisited. A comprehensive study of MoF_5.

Riane E. Stene [a,b], Benjamin Scheibe [a], Clemens Pietzonka [a], Antti J. Karttunen [c], Winfried Petry [b] and Florian Kraus [a,*]

Dedicated to Professor Erhard Kemnitz to further acknowledge his ACS Award for Creative Work in Fluorine Chemistry

[a] Anorganische Chemie, Fachbereich Chemie, Phillips-Universität Marburg, Hans-Meerwein-Straße 4, 35032 Marburg, Germany
[b] Department of Physics, Technische Universität München, Lichtenbergstraße 1 85748 Garching, Germany
[c] Department of Chemistry and Material Science, Aalto University, 00076 Aalto, Finland
* Correspondence: florian.kraus@chemie.uni-marburg.de; Tel.: +49 6421 28 26668

Academic Editor: name
Received: date; Accepted: date; Published: date

Abstract: While the properties of molybdenum pentafluoride, MoF_5, have been investigated in the past, there exists no comprehensive study of the compound. Additionally, many of these studies appear incoherent and offer contradictory explanations of some of the observed properties of MoF_5. Consequently, a comprehensive examination of MoF_5 is presented here, including a redetermination of the crystal structure of MoF_5 using single crystal and powder X-ray diffraction, the reevaluation of its IR, Raman and UV-vis spectrum, and a study of its density (3.50(2) g/cm^3 @ 25 °C) and magnetic properties. Additionally, density functional theory (DFT) calculations were performed on the gas phase molecule Mo_4F_{20} to provide a discussion of properties realized during investigation. Single crystal X-ray diffraction showed MoF_5 to crystalize in the monoclinic, *C*2/*m* space group, as isolated tetramers having the formula Mo_4F_{20}. Magnetic measurements showed that when "MoF_5" is cooled from the melt fast enough, paramagnetic species with $S = ½$ are present together with S = 0 species. These species may be described using the formula $(MoF_5)_n$ (n = odd) and $(MoF_5)_n$ (n = even, presumably $n = 4$). From the measurements, the content of the $S = ½$ species is estimated to be 6 %. The preferred species of MoF_5 under ambient conditions is Mo_4F_{20}.

Keywords: crystal structure; IR spectroscopy; UV-vis spectroscopy; Raman spectroscopy; density; magnetic properties; molybdenum; fluoride; MoF_5 type; WOF_4 type

---

1. Introduction

The synthesis of molybdenum pentafluoride was first described by R. D. Peacock in 1957 as a result of passing dilute fluorine gas over molybdenum hexacarbonyl at −75 °C to produce Mo_2F_9, which decomposes at 170 °C under vacuum to give MoF_5 and MoF_4 [1]. However, due to the use of fluorine gas, this reaction was described by preceding authors as quite exothermic. Since, simpler techniques have been discovered to produce MoF_5, such as the method used in this work which was briefly described by Geichman and coworkers [2] and which will be elaborated upon here. In short, MoF_6 is reduced using carbon monoxide and ultraviolet radiation. After the volatile products are discarded, pure MoF_5 can be collected from the reaction vessel.

MoF_5 is a sunflower yellow powder which, at high purities, melts at 45.7 °C (318.9 K) [3] and reacts with moisture to give a blue hydrolysis product, likely belonging to the molybdenum blues class of compounds. However, other sources report the melting point of MoF_5 to be between 63 and 67 °C (336 – 340 K) [1,4,5] but our observations are in agreement with the lower reported melting point.

MoF_5 is reported to be soluble in anhydrous HF without decomposition [5], however, through this work it has been found that, while MoF_5 is stable in anhydrous HF, it has limited solubility in

the solvent at room temperature. It sublimes at 50 °C [5] and disproportionates at 165 °C, giving MoF_4 and MoF_6 [4], however, no atmospheric or pressure conditions were reported for these measurements. Interestingly, though, mass spectroscopic and electron-diffraction studies on overheated vapors of MoF_5 report the molecule to be stable at temperatures as high as 280 °C [6,7]. Additional properties of MoF_5 have been reported, albeit not a lot of work has been done on MoF_5 since the 1970's. UV-Vis [8], IR [9,10], and Raman data [9–11] are available for MoF_5, however, little to no explanation of the bands arising from these spectra is given in these works. The magnetic properties and electronic properties [12–14], vapor pressure curve [4], and other thermodynamic properties [3] of MoF_5 have also been studied.

Edwards and coworkers investigated the crystal structure of MoF_5 in 1962 [15]. However, they state "the intensities of the spots (collected from single crystal oscillation and Weissenberg photographs) were difficult to estimate" and that the observed differences of Mo1—$F_{terminal}$ and Mo2—$F_{terminal}$ bond lengths are "probably not significant". In our efforts to explore the chemistry of MoF_6 and MoF_5 in greater detail, we obtained single crystals of the latter and re-determined its crystal structure to a much higher accuracy. We also set out to describe the properties of the absorption spectra of MoF_5, and elaborate upon the magnetic measurements already described in the literature. Additionally, the density of MoF_5 was investigated and is reported here.

2. Results and Discussion

2.1 Single-crystal and powder X-ray structure analysis

MoF_5 crystalizes as fluorine-bridged tetramers having the formula Mo_4F_{20} (M = 763.76 g/mol). Single crystal X-ray diffraction showed the crystal structure of MoF_5 as belonging to the monoclinic space group *C*2/*m* (no. 12). The lattice parameters of MoF_5 were calculated by LeBail refinement from a powder diffraction measurement taken at room temperature: a = 9.6502(2), b = 14.2451(2), c = 5.3100(1) Å, β = 93.088(1)°, V = 728.89(2) Å^3. These lattice parameters are in good agreement with those obtained by Edwards and coworkers (a = 9.61(1), b = 14.22(2), c = 5.16(1) Å, β = 94.21(20)°, V = 703 Å^3) [15], however, no measurement temperature was reported for their data collection. The powder diffraction pattern of MoF_5 in Figure 1 shows the synthesized compound to be phase pure; the crystal parameters for MoF_5 are listed in Table 1.

MoF_5 crystallizes in the MoF_5 structure type (m*S*48, *C*2/*m*) which is sometimes referred to as the WOF_4 structure type [16] and is characterized by MoF_5-units forming tetramers having the Niggli formula ${}^{0}_{\infty}[MoF_{2/2}F_{4/1}]$. The fluorine atoms in the crystal structure of MoF_5 pack in a distorted cubic closed packed array. An identical structural motif is observed in the compounds M_4F_{20} (M = Nb, Ta), whereas the M_4F_{20} structure found in the crystals of RuF_5, OsF_5, RhF_5 and PtF_5 (RuF_5 type, m*P*48, $P2_1/c$) is characterized by corrugated tetramers and fluorine atoms which pack in distorted hexagonal closed packed arrays. Moreover, the atomic distances and angles of MoF_5 are comparable to those of NbF_5 and TaF_5.

The crystal structure of MoF_5 can be seen in Figure 2 and the tetramer Mo_4F_{20} motif formed by MoF_5 is presented in Figure 3. In the specific case of Mo_4F_{20}, there are two distinct types of Mo atoms, one residing on the Wyckoff position 4*h* (site symmetry 2; Mo1) and the other residing on 4*i* (site symmetry *m*; Mo2). In both cases, the Mo atoms experience octahedron-like coordination by six fluorine atoms, in which two of these fluorine atoms are bridging to other Mo atoms. The atomic distance between Mo1 to the μ-bridging fluorine atoms F4, which reside on the 8*j* (1) positions, are observed to be 2.0423(11) Å, whereas the Mo2—μ-F distance is 2.0463(11) Å. Both agree well within the 3σ criterion. The μ-F—Mo—F_{trans} angles are essentially equal with a value of 178.04(6)° for Mo1 and 178.15(6)° for Mo2. Edwards and coworkers reported a Mo1—F4 distance of 2.04(4) Å and a slightly longer Mo2—F4 distance of 2.09(4) Å [15], both of which agree with our findings. However, their reported μ-F—Mo1—F_{trans} and μ-F—Mo2—F_{trans} angles are both 180.0(2)°.

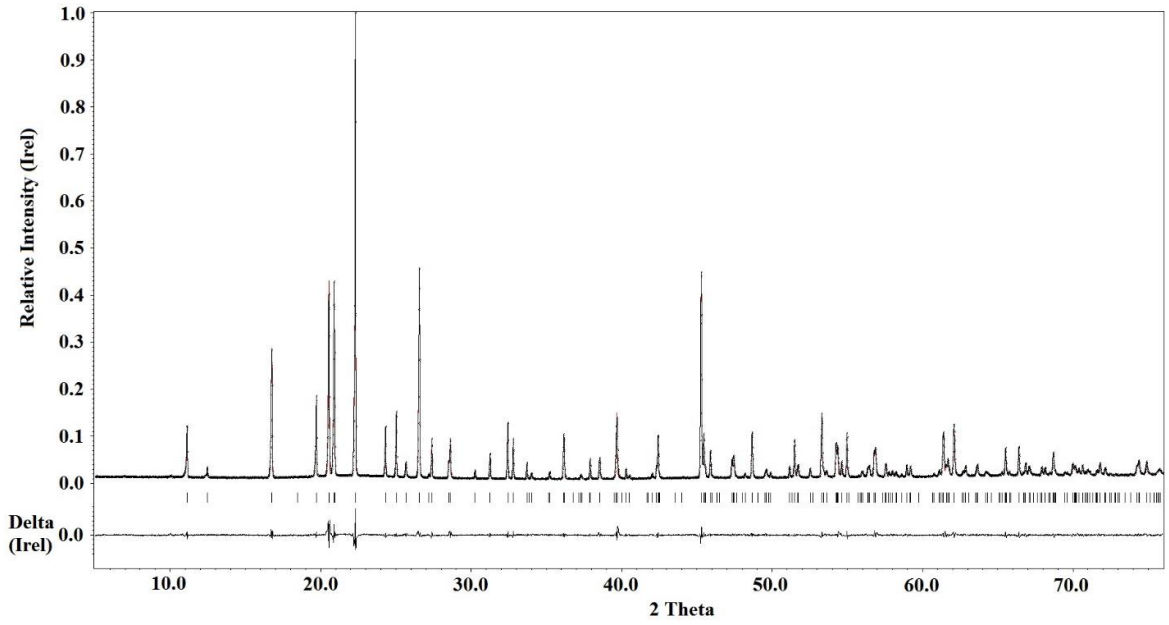

Figure 1. Powder diffraction pattern of MoF_5 measured at 293 K, processed through the Jana2006 program using a Le Bail refinement. The observed powder diffraction pattern is shown in black, while the calculated powder diffraction pattern is shown in red (barely visible due to good agreement). The difference between the observed and calculated patterns is shown by the black difference curve at the bottom of the schematic.

The atomic distances of Mo1—F5, Mo2—F1 and Mo2—F2, which are the distances to the so called axial F-atoms, are 1.8012(13), 1.8013(18) and 1.8011(18) Å, respectively, and are thus essentially identical. The distances of Mo1—F6 and Mo2—F3, where the respective F atoms are in trans position to the μ-F atoms and thus will be called equatorial F atoms, are slightly elongated with distances of 1.8236(14) and 1.8183(13) Å, respectively. Thus, the equatorial F atoms exhibit larger distances to the Mo atoms by about 0.02 Å in comparison to the axial F atoms (F1, F2, and F5). It is interesting to note that this finding may be a representation of the structural trans effect [17,18]. However, to the best of our knowledge this has not been reported for (pseudo)octahedral, homoleptic complexes. In NbF_5 and TaF_5 the distances of the metal atoms to the terminal F atoms are very similar, or the same, if the 3σ criterion is applied and no clear difference in length of the equatorial or axial bonds is observed. Thus, this structural trans effect may arise from the d^1 electron configuration of the Mo atoms and will be elaborated upon in the Computational Results section.

Interestingly, the Mo1—F6 bond length reported by Edwards and coworkers (1.89(4) Å) [15], is rather unprecise than that reported here (1.8236(14) Å). It is unclear why Edwards and coworkers observed such an elongation for the equatorial F atoms on the Mo1 atom but this may be due to the problems they described for the estimation of spot intensities. In contrast to this elongation, their reported Mo2—F3 bond length is significantly shorter with a distance of 1.74(4) Å. For the axial F atoms (F5 on Mo1 and F1 and F2 on Mo2), atomic distances of 1.82(9), 1.66(1), and 1.69(1) Å were reported, respectively [15]. In our case, 1.8012(13), 1.8013(18) and 1.8011(18) Å are observed for these respective atomic distances.

As may be expected, the Mo—F atomic distances for the terminal F-atoms are smaller in comparison to those of the bridging fluorine atoms (2.0423(11) and 2.0463(11) Å) by about 0.22 Å for those in equatorial position and 0.24 Å for the axial ones.

Table 1. Crystallographic parameters for MoF_5. The middle column outlines parameters collected from single crystal X-ray diffraction (SCXRD) while the second column outlines parameters collected from powder X-ray diffraction (PXRD).

	MoF_5 (SCXRD)	MoF_5 (PXRD)
empirical formula	MoF_5	MoF_5
color and appearance	transparent yellow cuboid	yellow powder
molecular mass [g/mol]	190.94	190.94
crystal system	Monoclinic	monoclinic
space group	*C*2/*m* (12)	*C*2/*m* (12)
a [Å]	9.4719(7)	9.6502(2)
b [Å]	14.1200(7)	14.2451(2)
c [Å]	5.0856(4)	5.3100(1)
β [°]	96.191(6)	93.088(1)
V [Å^3]	676.20(8)	728.89(2)
Z	8	8
ρ_{calc} [g cm^{-3}]	3.751 @ 100 K	3.4789 @ 293 K
ρ_{exp} [g cm^{-3}] @ 25 °C	—	3.50(2)
λ [Å]	0.71073 (MoK_α)	1.54051 (CuK_α)
T [K]	100	293
μ [mm^{-1}]	3.854 (MoK_α)	30.368 (CuK_α)
θ_{max}	34.856	—
2 θ range measured (min, max, increment)	—	5.007, 75.972, 0.015
2 θ range refined (min, max)	—	5.007, 75.972
hkl_{max}	$-15 \le h \le 15$	—
Size [mm^3]	0.13 × 0.12 × 0.17	—
R_{int}, R_σ	0.047	—
R (*F*) ($I \ge 2\,\sigma(I)$, all data)	0.0264, 0.0287	—
wR (F^2) ($I \ge 2\,\sigma(I)$, all data)	0.068,0.0693	—
Rp, *wRp*	—	0.0437, 0.0610
S (all data)	1.154	—
data, parameter, restraints	1511, 61, 0	4732, 23, 0
$\Delta\rho_{max}$, $\Delta\rho_{min}$ [e Å^{-3}]	1.08, −1.54	—

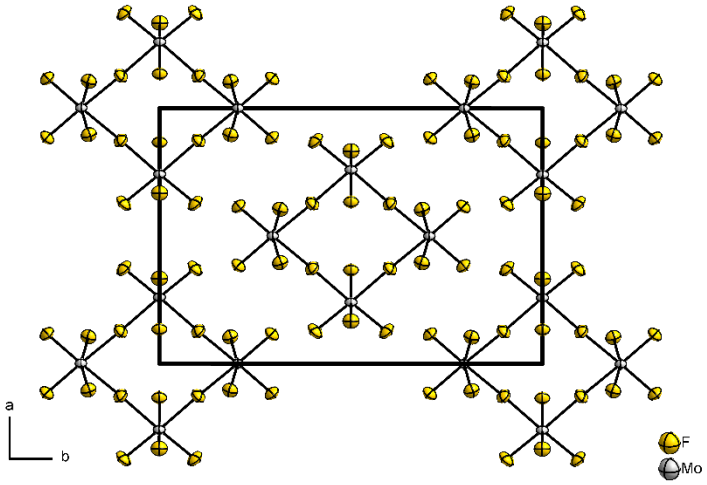

Figure 2. A section of the crystal structure of MoF_5 viewed along the *c*-axis. Displacement ellipsoids shown at the 70% probability level at 100 K.

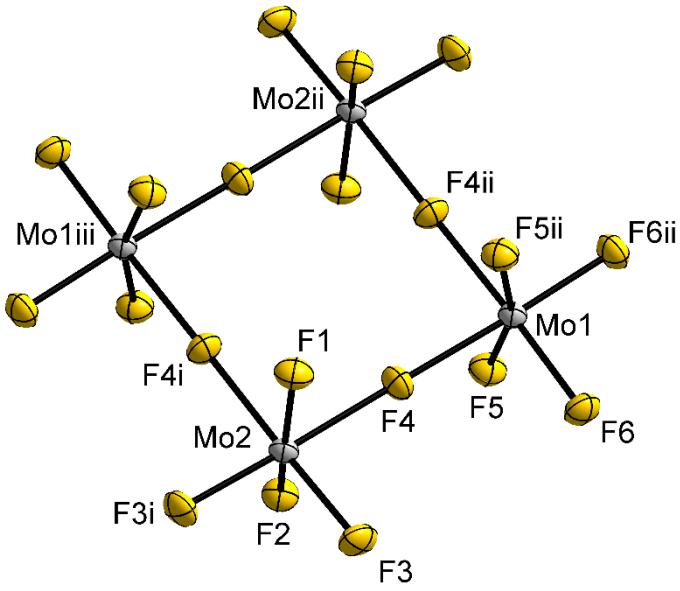

Figure 3. Structure of the MoF_5 tetramer unit displaying the MoF_4 units bridged through two fluorine atoms to two neighboring Mo atoms. Atom labeling in accordance to the manuscript by Edwards and coworkers [15]. Displacement ellipsoids are shown at the 70% probability level at 100 K. [Symmetry codes: (i) $x, -y, z$; (ii) $-x, y, 1-z$; (iii) $-x, -y, 1-z$.]

The point symmetry of the Mo_4F_{20} molecule is 2/*m*, C_{2h}, with the twofold rotation axis running through the Mo1 atoms and the perpendicular mirror plane bisecting the Mo2, F1 and F2 atoms. The Mo—Mo distance is 4.0881(3) Å, and the four membered ring formed by the Mo atoms is a flat square.

2.2. Electronic and Vibrational Spectroscopy

The electronic spectrum of MoF_5 dissolved in perfluoroether ($C_8F_{16}O$, FC-75, 3M) was studied in the range of 400 to 1100 nm (see Figure 4). The spectrum obtained was rather simple with absorption occurring in the near UV and blue regions (beginning at about 500 nm), and the

beginning of another absorption band starting at about 770 nm and extending into the near IR region of the spectrum. Peakcock and Sleight studied the electronic spectrum of molten MoF_5 in the region of 4000 to 26000 cm^{-1} (2500 to 385 nm) [8]. They observed a single band in the spectrum centered at 7500 cm^{-1} (1333 nm). The single absorption band found in the work of Peacock and Sleight may arise from the same electronic transition giving rise to the absorption in the red and near IR regions in this work, however, a direct comparison cannot be made since both works obtained spectra using different sample conditions.

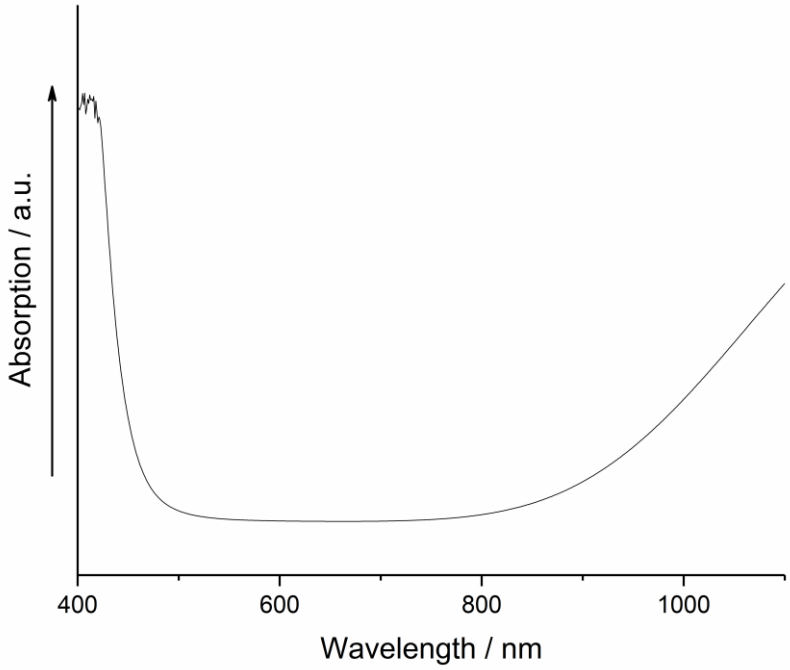

Figure 4. Visible and near IR spectrum of MoF_5 dissolved in perfluoroether.

IR spectroscopy was studied on a polycrystalline sample of MoF_5 at 25 °C in the region of 900 to 400 cm^{-1}. The IR spectrum obtained from this work shows five bands at approximately 762, 739, 720, 675 and 496 cm^{-1}. It can be said that the bands at 762, 739, 720 and 675 cm^{-1} are all overlapping to some degree. Upon comparison of the measured IR spectrum to that of a IR spectrum calculated for the solid state of MoF_5 using the DFT-PBE0 method (a more detailed description of these calculations can be found in the Computational Results section), it can be seen that the peak positions correlate very well, however, the peak shapes and intensities vary. A comparison of the experimental and theoretical spectra is shown in Figure 5. Furthermore, peak assignments for the bands in the experimental IR spectrum were made utilizing the results of the theoretically calculated IR spectrum in which the theoretical vibrations were visualized using the Jmol software [19]. Band assignments are listed in Table 2.

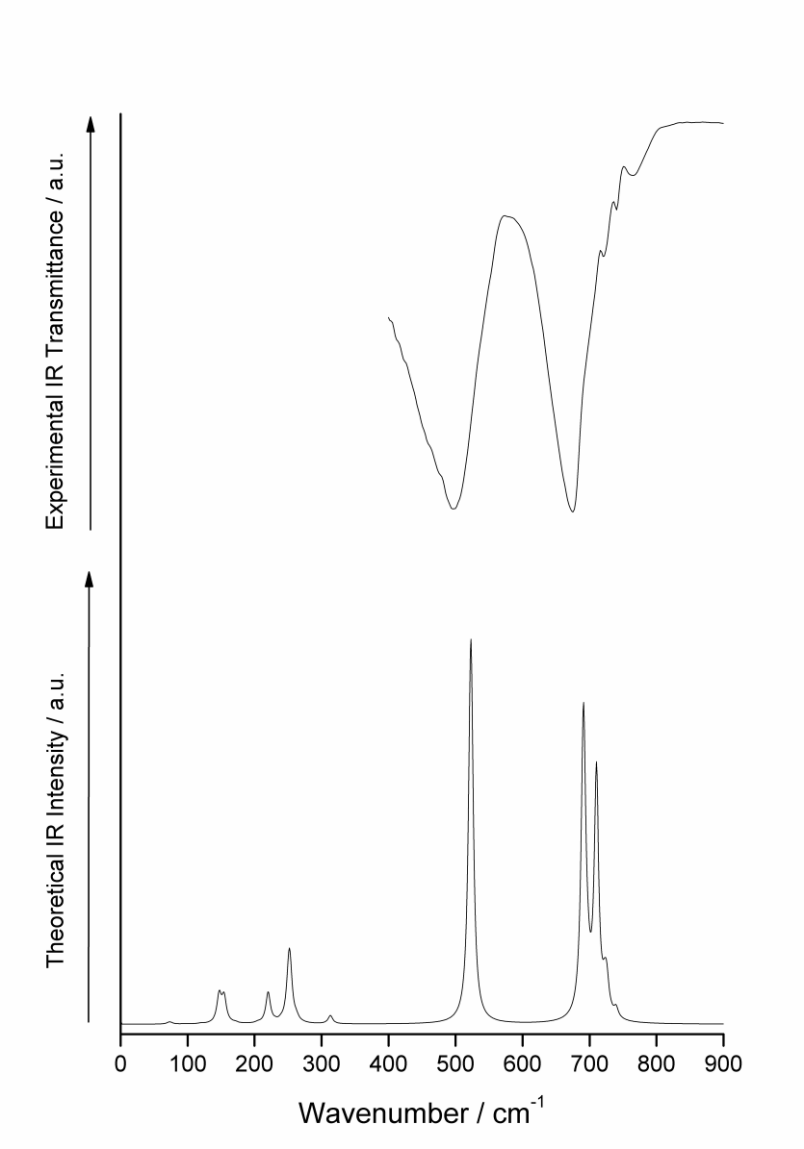

Figure 5. Top: Experimentally obtained IR spectrum of crystalline MoF_5; bottom: Theoretically calculated IR spectrum of the solid state of MoF_5 calculated using the DFT-PBE0 method.

As mentioned earlier, IR spectroscopy of MoF_5 has been previously studied. Acquista and Abramowitz studied differences in the IR spectra of MoF_5 vapors in argon matrices at liquid helium temperatures [9]. These differences occurred by allowing the MoF_5 vapors to reach equilibrium at different temperatures in the range of 25 – 150 °C before being trapped at liquid helium temperatures for measurement. They observed bands at 768, 716, 704 and 231 cm^{-1} during the room-temperature measurements. At higher temperatures, though, these bands began to decrease in intensity while bands at 713, 683, 261 and 112 cm^{-1} began to appear. They attributed this observation to the disappearance of polymeric species at higher temperatures and the increase of the monomeric MoF_5 unit. However, a comparison of these IR spectra in argon matrices to the polycrystalline spectrum reported here cannot be made due to the extreme differences in sample handling and measurement techniques. Acquista and Abramowitz also studied a solid-state spectrum of MoF_5 at liquid helium temperatures, which gave rise to broad bands at 725, 700, 660, and 525 cm^{-1} [9]. Due to its absence in the spectra of heated samples described above, they attributed the band at 525 cm^{-1} as arising from the fluorine-bridge bond of the tetrameric unit. This band at 525 cm^{-1} may correspond to the band observed in this work at 496 cm^{-1}, which arises from the symmetric and asymmetric stretching of the Mo—μ-F bonds, in which case the observations of Acquista and Abramowitz may be confirmed. However, the solid-state spectrum of MoF_5 received

from Acquista and Abramowitz [9] is completely different from that reported in this work. This difference, however, may arise from different sample handling techniques and temperature of analysis.

Ouellette and coworkers studied the IR spectrum of a super-cooled liquid of MoF_5 at 25 °C [10]. This spectrum showed bands at approximately 725, 690, 490, 250, 180 and 130 cm^{-1}. Analysis of their liquid MoF_5 data was made on the assumption that monomeric MoF_5 species (of D_{3h} symmetry) were present in their melted sample. The liquid IR spectrum obtained from the work of Ouellette and coworkers has similar features when compared to the polycrystalline spectrum obtained in this work, although the peak positions and intensities are different. They also studied the IR spectrum of solid MoF_5 which showed weak bands at 970, 890, 845, 520 and 480 cm^{-1}, medium bands at 200 and 160 cm^{-1}, and very strong bands at 745, 698 and 647 cm^{-1}. The authors did not attempt to make band assignments for the spectrum of solid MoF_5 due to the complexity of the molecule's solid state structure, nor do they state the temperature at which the measurement was performed. Nevertheless, similar features can also be seen in their solid MoF_5 spectrum when compared to the polycrystalline spectrum reported here. The IR bands obtained from this work and previous works can be compared in Table 2.

Furthermore, an interesting statement was found in the work of Ouellette and coworkers [10] in which they report the unlikelihood that a reversible change between the tetrameric unit in the solid and a polymeric unit ($n > 4$) in the liquid could be made [10]. This statement was tested in this work through the use of IR spectroscopy to determine if a crystalline sample of MoF_5 decomposes after several melting and cooling cycles to a glassy state characterized by an increased presence of monomers, dimers, or trimers. In this experiment, a sample of MoF_5 was melted at 90 °C and then immediately cooled in liquid nitrogen to produce glassy MoF_5. It was observed that this glassy product quickly reverted back to the crystalline form at room temperature within minutes. Sequential IR spectra taken after nine melting, cooling and annealing (at room temperature) cycles looked identical to the one shown in Figure 5; no new peaks appeared in the range measured. This suggests that any polymeric species present in the melt either recombine or decompose to form the tetramer unit at room temperature. However, our magnetic measurements (see below) showed that cooling rates are of great importance in the conservation of the $(MoF_5)_n$ species.

Lastly, a Raman spectrum was obtained for a crystalline sample of MoF_5 at room temperature (see Figure 5). This spectrum showed eleven discernible bands at 757, 736, 703, 694, 401, 288, 248, 239, 197, 181 and 134 cm^{-1}. It was compared to a theoretically calculated spectrum obtained for the solid state of MoF_5 using the DFT-PBE0 level of theory. These spectra can be compared in Figure 6. The band locations correlate very well between the experimental and theoretical spectra, however, the band intensities are different. A peak at 401 cm^{-1} is present in the experimentally obtained Raman spectrum but absent in the theoretically calculated spectrum. This peak may be an overtone of two vibrational modes, or it may arise from a small amount of polymers and/or monomers in the sample, or from an impurity. Band assignments were made using the theoretical Raman spectrum and can been seen in Table 2. Raman spectroscopy of crystalline MoF_5 has previously been studied by Acquista and Abramowitz [9], Ouellette and coworkers [10], and Bates [11]. The spectrum obtained from this work agrees very well with the spectra obtained from these previous studies; they can be compared in Table 2.

Table 2. Comparison of IR and Raman data obtained in this work and previously reported works [9–11]. Band assignments are given for the IR and Raman spectrum obtained from this work (ν = vibration; δ = deformation; ρ_r = rocking; ρ_t = twisting). Where two or more band assignments are given, coupling of these optical modes were obtained from the quantumchemical calculations. Some vibrational assignments are reported without a ''symmetrical'' or ''asymmetrical'' classification due to overlap.

This work IR (crystalline) [cm^{-1}]	Acquista et al. IR (solid) [cm^{-1}]	Acquista et al. IR (argon matrix) [cm^{-1}]	Ouellette et al. IR (solid) [cm^{-1}]	Ouellette et al. IR (liquid) [cm^{-1}]	This work Raman (crystalline) [cm^{-1}]	Acquista et al. Raman (crystalline) [cm^{-1}]	Ouellette et al. Raman (crystalline) [cm^{-1}]	Bates Raman (crystalline) [cm^{-1}]
			970					
			890					
			845					
762 ν_s(Mo—F_{eq})	725	768	745	725	757 ν_s(Mo—F_{eq});	758	759	759
739 ν(Mo—F_{ax});	700	735			ν_{as}(Mo—F_{ax})	746	746	747
ν_{as}(Mo—F_{eq})*		733			736 ν_s(Mo—F_{ax});	736	737	738
720 ν(Mo—F_{ax});		716			ν_s(Mo—F_{eq})	704	704	706
ν(Mo—F_{eq})		713			703 ν_{as}(Mo—F_{eq});			
		704			ν_{as}(Mo—F_{ax})			
675 ν_s(Mo—$F_{terminal}$);	660	683	698	690	694 ν_{as}(Mo—F_{eq});	696	696	696
ν_{as}(Mo—$F_{terminal}$)*			647		ν_s(Mo—$F_{terminal}$)*	683		684
	525		520				563	
496 ν_s(Mo—μ-F);			480	490	401	494	406	494
ν_{as}(Mo—μ-F)*						400		436
								402
								332
		261	200	250	288 δ(F_{eq}—Mo—F_{eq});	288	294	282
		231			δ(μ-F—Mo—μ-F)	250	250	252
					248 δ(F_{eq}—Mo—F_{eq})	236	241	239
					239 δ(F_{eq}—Mo—F_{ax})			
		112	160	180	197 ρ_r(F_{ax}—Mo—F_{ax});	198	198	199
				130	ρ_r(F_{eq}—Mo—F_{eq});	181		181
					δ(F_{eq}—Mo—F_{eq})*	127		
					181 δ(μ-F—Mo—μ-F);			
					ρ_t(F_{ax}—Mo—F_{ax})			
					134 ρ_t(F_{eq}—Mo—F_{eq});			
					ρ_t(μ-F—Mo—μ-F);			
					ρ_r(F_{ax}—Mo—F_{ax})			
						59		

*Indicates two vibrational modes which occur so closely to each other that they could not be resolved into two peaks

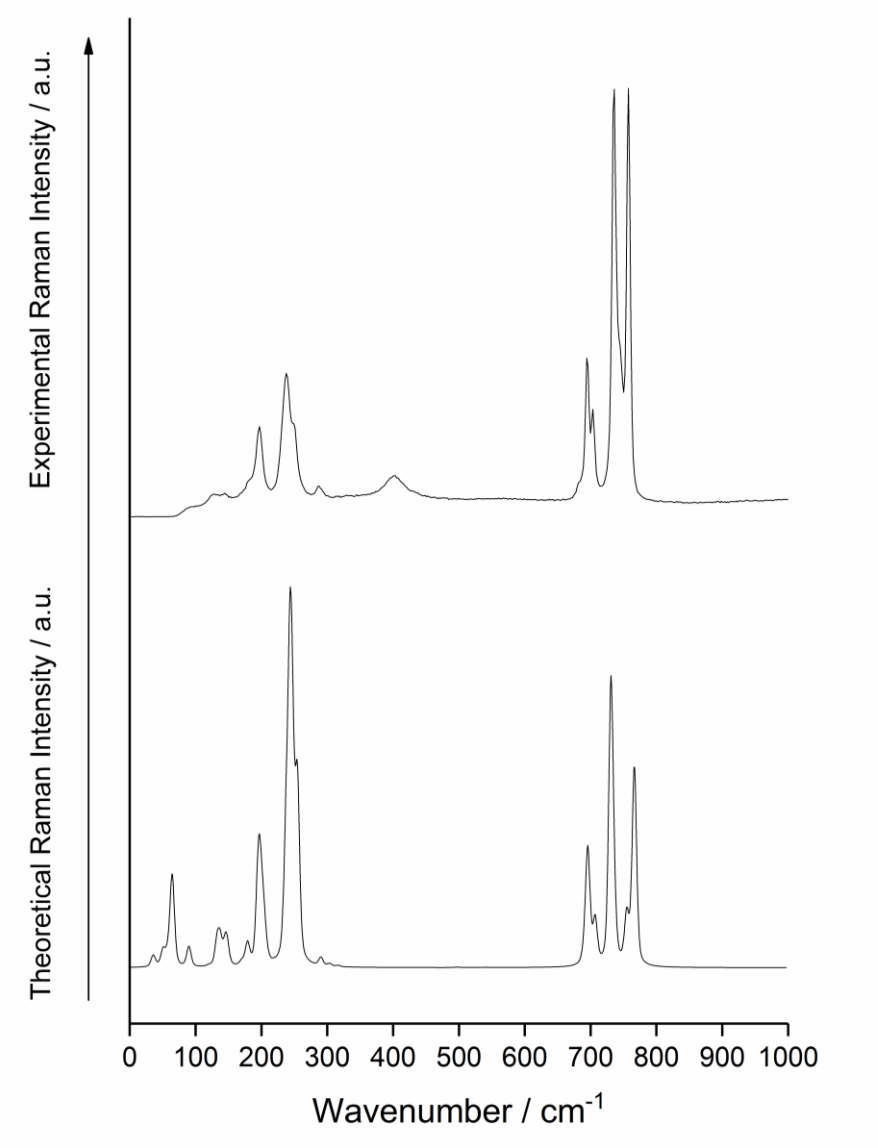

Figure 6. Top: Measured Raman spectrum of crystalline MoF_5; bottom: Theoretical Raman spectrum of the solid state of MoF_5 calculated using CRYSTAL17 calculations.

2.3. Magnetic Measurements

Magnetic data of MoF_5 was obtained with the application of the VMS option of a Quantum Design physical property measurement system (ppms). The material had to be measured in a homemade FEP sample holder due to the enhanced reactivity of MoF_5 with moisture residues present in traditional sample holders. The data was corrected with respect to the contribution of the sample holder as well as the diamagnetic contribution of the sample through utilization of both experimental data and Pascal constants. The molar diamagnetic susceptibility of MoF_5 was calculated to be $-6.8 \cdot 10^{-5}$ cm^3 mol^{-1}. Field and temperature dependent magnetic data was also recorded.

Temperature-dependent scans with applied fields of 1 and 5 Tesla were performed in the temperature range from 1.8 K to 300 K. The curves show a broad maxima at about 260 K. A decrease in temperature is met with decreasing magnetization, however, at temperatures below 50 K, the magnetization increases once again and reaches values close to the room temperature measurements (see Figure 7).

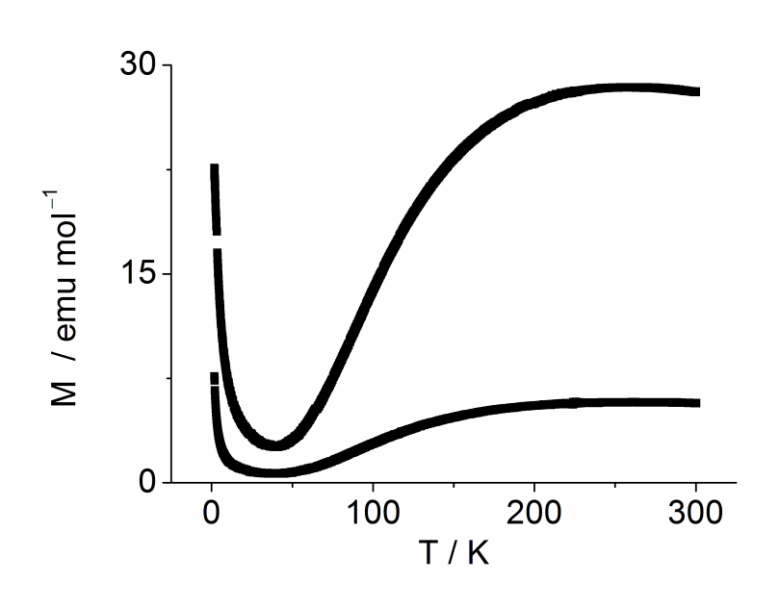

Figure 7. Magnetization curve of "MoF_5" at 1 (lower curve) and 5 T (upper curve).

Field-dependent measurements of MoF_5 were also carried out at 1.8, 5, 10, 15, 50, 100, 150, 200 and 300 K. Up to 10 K the magnetization data show significantly sigmoidal curves. Above 10 K the behavior is linear (Figure 8 and Figure S1).

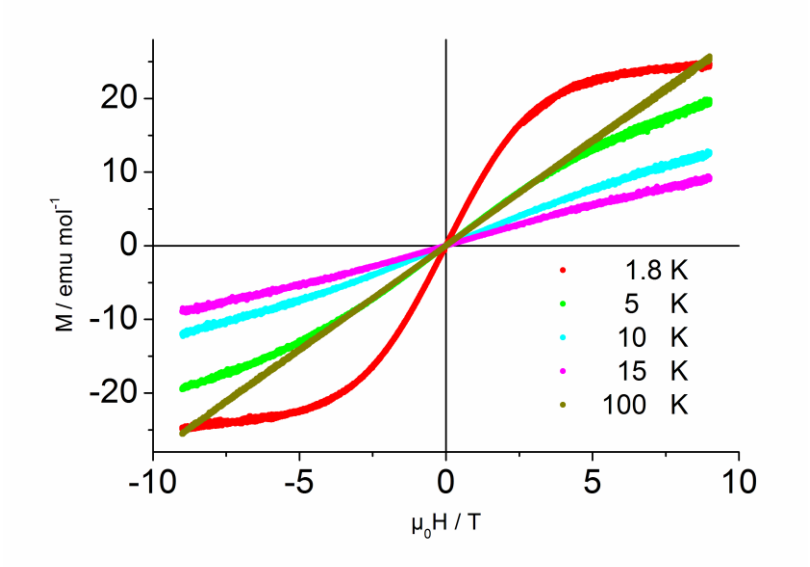

Figure 8. Field dependent measurements on a crystalline sample of MoF_5.

This data describes the magnetic behavior of the crystalline state of MoF_5, which is in good agreement with the previously reported [14] antiferromagnetism of MoF_5 that is responsible for the observed maximum at 260 K. The increase of the magnetization below 50 K is an indicator towards the presence of an additional paramagnetic phase in the sample. This observation indicates the breakdown of the Mo_4F_{20} unit into smaller subunits (i.e. monomers, dimers, and trimers). If the paramagnetic behavior is assumed to stem from species with $S = ½$, that is, $(MoF_5)_n$ (n = odd) subunits, their amounts can be estimated to circa 0.3% for $n = 1$, and circa 1% for $n = 3$. These amounts were determined based on the Brillouin-fit shown in Figure S1. Such amounts are not observable, or would be very difficult to observe, in a powder X-ray diffraction pattern, so it is unclear whether the paramagnetic phase is crystalline or amorphous. However, due to the observed

ability of MoF_5 to be readily super-cooled [10] and easily transferred to an amorphous state [14], we assume it to also be amorphous in our case.

This cooled MoF_5 sample was then warmed above its melting point, leading to an increase in the observed magnetization. The rise in the magnetization curve observed at approximately 321 K is, however, dependent upon the heating rate, as shown in Figure 9. In all cases, though, the content of the paramagnetic species with $S = ½$ seems to have increased abruptly to approximately 6% (Brillouin-fit in Figure S1), indicating cleavage of the tetramer unit. Upon rapidly cooling the heated sample (20 K/min, indicated by blue curve in Figure 9) a retainment of these paramagnetic species seems to occur, as indicated by an observed Curie-Weiss-like magnetic behavior. A Curie-Weiss-fit (Figure S2) yielded a θ value of −141.7(2) K, indicating the presence of somewhat strong antiferromagnetic coupling within this phase. If a Curie-Weiss-fit with two phases, one being a putatively strong antiferromagnetic phase and the other being a paramagnetic phase, is carried out, then the ratio of these two phases can be determined, leading to the calculation of approximately 6% paramagnetic, $S = ½$ species present in the sample.

Upon warming of this increased-paramagnetic, metastable phase to 300 K, with a heating rate of 2 K/min, a recombination of the $(MoF_5)_n$ species (with n = odd) to $(MoF_5)_n$ (with n = equal; most likely $n = 4$) is likely occurring as indicated by the decrease in susceptibility to the former value of the crystalline phase (as shown by the violet curve in Figure 9). As we cannot observe the sample visually during the magnetic measurements, it remains an open question as to whether the increase in paramagnetic species corresponds to the melting of the compound, or if the tetramers begin to decompose in the solid state. However, melting of the sample is suspected as the temperature nicely corresponds to the reported melting point of high purity MoF_5 [3].

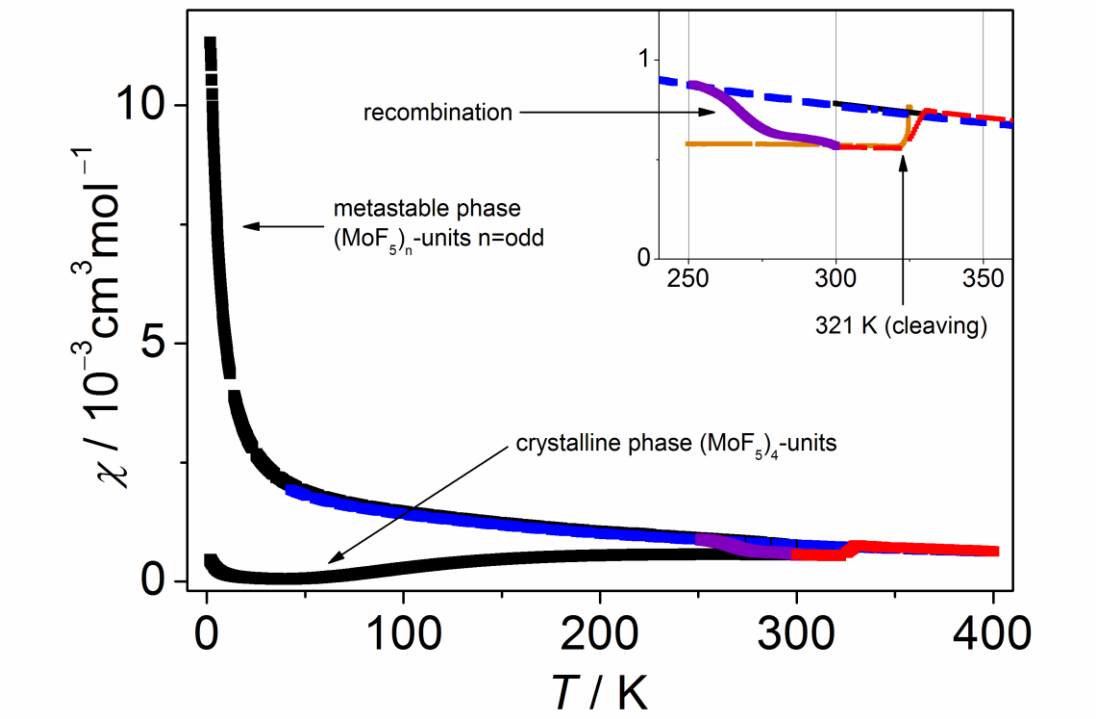

Figure 9. Magnetic susceptibility of two different MoF_5 phases (black). The magnetic behavior during the phase transitions is measured with rising temperatures. The cleavage of the tetramers is shown by the red and orange curves (two separate measurements), the recombination of $(MoF_5)_n$ (n = odd) to $(MoF_5)_n$ (n = equal; very likely $n = 4$) is shown by the violet curve. The rapid cooling of the

heated sample with a cooling rate of 20 K/min, which presumably leads to an amorphous state, is shown by the blue curve.

2.4 Computational Results

Solid MoF_5 (Mo_4F_{20}) was investigated at the DFT-PBE0/TZVP level of theory (see Materials and Methods for full computational details). First, the geometries of two spin configurations were fully optimized, corresponding to the spins of the four Mo atoms in either a ferromagnetic (FM) or antiferromagnetic (AFM) configuration. Both spin configurations could be studied in the original space group *C*2/*m*. The AFM configuration turned out to be the magnetic ground state, being 5 kJ/mol lower in energy in comparison to the ferromagnetic configuration. The absolute value of the spin-only magnetic moment of the Mo atoms is 0.94 μ_B. All solid-state results discussed below have been obtained for the antiferromagnetic ground state.

The lattice parameters of the optimized crystal structure are slightly overestimated in comparison to the SCXRD structure (differences in parentheses): a = 9.74 Å (2.8%), b = 14.39 Å (1.9%), c = 5.21 Å (2.5%) and β = 95.9° (–0.3%). The calculated Mo–F distances showed the same trend as observed in the experimental structure: Mo–F_{bridge} = 2.07 Å, F_{eq} = 1.84 Å, and F_{ax} = 1.82 Å. The IR and Raman spectra calculated for MoF_5 are shown in Figure 5 and Figure 6, respectively. The calculated spectra are in good agreement with the experimental spectrum and enabled the assignment of the vibrational modes.

In addition to solid-state MoF_5, the Mo_4F_{20} molecule was investigated in the gas-phase (DFT-PBE0/def2-TZVP level of theory). The D_{2h}-symmetric antiferromagnetic ground state is 7 kJ/mol more stable than the D_{4h}-symmetric ferromagnetic spin configuration. We investigated the chemical bonding with the help of Intrinsic Atomic Orbital (IAO) population and Intrinsic Bond Orbitals (IBOs) analysis. The partial atomic charges (e^-) are as follows: Mo = +2.09, F_{bridge} = –0.55, F_{eq} = –0.40, and F_{ax} = –0.37. The larger the partial charge of an F atom, the longer the calculated Mo–F distance: Mo–F_{bridge} = 2.06 Å, F_{eq} = 1.82 Å, and F_{ax} = 1.80 Å. The longer Mo–F_{eq} distance in comparison to Mo–F_{ax} distance is in agreement with the experimental and computational solid-state results. The elongation of the Mo–F_{eq} can be understood by analyzing the Mo–F bonding in terms of IBOs, which are a physically well-defined form of localized molecular orbitals (MOs) and more suitable for chemical interpretation than the delocalized canonical molecular orbitals. The IBO analysis shown in Figure S3 shows that the highest-energy lone pair orbital of the F_{eq} atom is in complete anti-phase to the Mo $d_{x^2-y^2}$ orbital (unpaired Mo d^1 electron). In the case of the F_{ax} atom, the highest energy lone pair orbital and the Mo $d_{x^2-y^2}$ orbital are not in complete anti-phase and some constructive overlap arises (the IBO has ~10% contribution from Mo). As a consequence, the repulsion between the Mo d^1 electron and the F lone pair electrons is smaller for the F_{ax} atoms than the F_{ex} atoms and the Mo–F_{ax} distance is slightly shorter than the Mo–F_{eq} distance.

The energetics of the following $(MoF_5)_n$ species were also studied (molecular geometries are included in the Supporting Information): MoF_5 (C_s); Mo_2F_{10} (D_{2h}); Mo_3F_{15} (D_{3h}); Mo_4F_{20} (D_{4h}); Mo_5F_{25} (D_{5h}). These were gas-phase calculations at 0 K and a ferromagnetic spin configuration was used for all systems since the aim of the study was to understand the structural strain in $(MoF_5)_n$ species and not to investigate the much smaller FM/AFM energy differences. This study gave the relative energies (kJ/mol) per MoF_5 unit, which for n = 1–5 are as follows: 67, 85, 41, 0, and 40. Thus, the concatenation of MoF_5 units is energetically favorable and the Mo_4F_{20} species is clearly the $(MoF_5)_n$ species with the smallest structural strain.

3. Conclusions

MoF_5 was synthesized by the reduction of MoF_6 in the presence of CO under UV irradiation. It was confirmed that MoF_5 crystallizes in the monoclinic *C*2/*m* space group as Mo_4F_{20} tetramers. Single crystal analysis showed a discernable difference in atomic distance between the Mo—F_{eq} and

the Mo—F_{ax} bonds, with the Mo—F_{eq} atomic distances being longer by about 0.02 Å. Theoretical calculations of the Mo_4F_{20} molecule in the gas-phase (run at the DFT-PBE0/def2-TZVP level of theory) were analyzed using IAO and IBOs. The IBO analysis showed the highest-energy lone pair orbital of the F_{eq} atoms to be in complete anti-phase with the Mo $d_{x^2-y^2}$ orbital, whereas the highest energy lone pair orbital of the F_{ax} atoms are not in complete anti-phase with the Mo $d_{x^2-y^2}$ orbital and instead exhibit some constructive overlap. This constructive overlap between orbitals in the Mo—F_{ax} bond is what leads to the slightly shorter bond length of this bond when compared to the Mo—F_{eq} bond.

Furthermore, the vibrational spectroscopy study of MoF_5 showed that great differences in the IR spectrum of the molecule can be observed depending on the sample handling and measurement techniques. Polycrystalline IR and Raman spectra are reported here, in which theoretical calculations of solid-state MoF_5 were used to make band assignments. It was shown that of the 69 possible optical modes of Mo_4F_{20}, 29 optical modes (18 Raman; 11 IR) could be seen in the computational spectra and 16 (11 Raman; 5 IR) could be seen in the experimental spectra. Band assignments for the experimental spectra can be seen in Table 2.

The study of the magnetic properties of a polycrystalline sample of MoF_5 showed the compound to exhibit antiferromagnetic properties, with a maximum observed at 260 K. An increase in magnetism was also observed at temperatures below 50 K. This increase in magnetism is thought to occur from paramagnetic $(MoF_5)_n$ (n = odd) subunits with S = ½. Warming of the sample lead to an increase of these S = ½ subunits, most likely belonging to the monomers and trimers of cleaved Mo_4F_{20} units. Upon rapid cooling of this sample with increased-paramagnetic behavior, it was shown that this increase in paramagnetism could be preserved. However, upon heating of this increase-paramagnetic, metastable phase back to room temperature, a decrease in magnetism was observed, leading to the conclusion that the paramagnetic, $(MoF_5)_n$ (n = odd), species recombined to give the Mo_4F_{20} tetramers. In support of this conclusion, it was shown through our computational study that the Mo_4F_{20} unit is the preferred species of ''MoF_5''. It seems a fair assessment to conclude from our investigations that, while a small percentage of MoF_5 may be found in the solid state as $(MoF_5)_n$ (n = 1-3) units, the preferred species of MoF_5 under ambient conditions is Mo_4F_{20}.

4. Materials and Methods

4.1. General Procedures and Materials

All operations were performed in either stainless steel (316L) or Monel metal Schlenk lines, which were passivated with 100% fluorine at various pressures before use. Preparations were carried out in an atmosphere of dry and purified Argon (5.0, Praxair). Carbon monoxide (5.0, Air Liquide Deutschland) was used as supplied. Molybdenum hexafluoride (99%, ABCR) was distilled once prior to usage. Several UV light bulbs (254 nm, HNS S 11 W G23, Osram Puritec) were used in a homemade chamber to promote MoF_6 reduction.

4.2. Synthesis of MoF_5

In order to synthesize molybdenum pentafluoride, MoF_6 (3.74 g, 17.80 mmol) was distilled into a 300 mL quartz vessel that was previously evacuated and flamed-dried three times. To this vessel 800 mbar (9.69 mmol) of carbon monoxide was added and the reaction vessel was placed into a chamber to allow irradiation by ultraviolet light (254 nm). After 12 hours of irradiation, the product was cooled using liquid nitrogen, the gaseous species in the vessel were evacuated, 800 mbar of fresh carbon monoxide was added, and the vessel was irradiated with UV light for an additional 12 hours. After the reaction was complete, all remaining volatile species were evacuated at room temperature and the product (a yellow powder) was transferred into a glovebox for further sample handling. The yield of MoF_5 was quantitative, except for mechanical losses. A powder X-ray

diffraction pattern was taken directly from the product with no further sample preparation and confirmed that phase-pure MoF_5 was obtained. The product was found to decompose in air to form a blue hydrolysis product, as expected.

In an inert atmosphere, about 200 mg of MoF_5 was transferred to an FEP (fluorinated ethylene propylene) tube and sealed. This tube was placed in an oil bath set to 90 °C in order to melt the sample. Once melted, the MoF_5 was allowed to slowly reach room temperature. This method was used to produce the single crystals used in this study. All other measurements of MoF_5 were performed directly on the powder obtained from the reaction.

4.3. Single Crystal X-ray Diffraction

X-ray structure analysis of the single crystals of MoF_5 was carried out with a STOE IPDS 2T diffractometer with plane graphite-monochromated molybdenum radiation (Mo-K_α, λ = 0.71073 Å) generated by a sealed X-ray tube (12×0.4 mm long fine focus), and a detector resolution of 6.67 pixels mm^{-1}. Evaluation and integration of the diffraction data was carried out using the X-Area software, and an absorption correction was made through integration using the X-Red[32] and X-Shape program within the parent software [20]. The structure was solved using the previous structure model of MoF_5 and refined against F^2 in the SHELXLE software [21,22]. All atoms were located by Difference Fourier synthesis and refined anisotropically. Representations of the crystal structure were created using the Diamond software [23]. Further details of the crystal structure investigation may be obtained from the Fachinformationszentrum Karlsruhe, 76344 Eggenstein-Leopoldshafen, Germany (Fax: +49-7247-808-666; E-Mail: crysdata@fiz-karlsruhe.de, http://www.fiz-karlsruhe.de/request for deposited data.html) on quoting the depository numbers CSD-433190.

4.4. Powder X-ray Diffraction

Powder X-ray diffraction patterns were obtained with a Stadi-MP-Diffractometer (STOE) using Cu-K_α radiation (λ = 1.54051 Å), a germanium monochromator, and a Mythen1K detector. The data were handled using the WINXPOW software [24]. The compound was filled into borosilicate capillaries, which were previously flamed dried under vacuum, and sealed using a hot tungsten wire. The powder diffraction pattern presented in this work was obtained using a ring collimator, a step size of 0.195° 2θ, and a measurement time of 125 seconds per step between 0 and 78° 2θ. Using the Jana2006 software [25], a Le Bail refinement was used to fit the powder diffraction pattern. A Chebyshev polynomial employing 15 terms was used for background correction, however, 3 of these 15 terms were omitted from refinement. In order to fit peak shape, a Pseudo-Voigt function was employed. Asymmetry was corrected through divergence.

4.5. UV/VIS Spectroscopy

The electronic spectrum was measure on a SPECORD 210 PLUS UV/Vis spectrophotometer. The sample was dissolved in perfluoroether and placed into a homemade sample holder with sapphire windows. The spectrum was processed with the WinASPECT Plus software [26].

4.6. IR Spectroscopy

The IR spectrum was measured on an alpha FTIR spectrometer (Bruker) using a diamond ATR unit under an Ar atmosphere. The spectrum was processed with the OPUS software package [27].

4.7. Raman Spectroscopy

MoF_5 was loaded into a 0.3 mm borosilicate capillary and the Raman spectrum was measured in backscattering geometry by means of a Raman microscope inVia (Renishaw), using a frequency-

doubled Nd:YAG laser (532 nm wavelength). The spectrum was recorded in confocal mode between 2 cm^{-1} and 1792 cm^{-1}. The laser power was reduced to 5% to prevent degradation of the sample.

4.8. Density Determination

The density of MoF_5 was measured using the automated gas displacement pycnometry system AccuPyc II 1340 (micromeritics) with a calibrated 0.1 cm^3 sample holder and helium as the displacement gas. The number of preliminary purges was set to 30, while the subsequent density measurements were performed 50 times with measurement averaging.

4.9. Magnetic Measurements

DC-magnetic data were recorded with the VSM option in a Physical Property Measurement System (PPMS Dynacool, Quantum Design, SanDiego, USA). Temperature and field dependent scans were performed in the range from 1.8 to 400 K and from −9 to 9 Tesla. The maximum cooling rate of 20 K/min allows to convert the MoF_5 from its liquid to a super-cooled state.

4.10. Computational details

Periodic quantum chemical calculations for MoF_5 were carried out using the PBE0 hybrid density functional method (DFT) [28,29]. A polarized triple-zeta-valence (TZVP) level basis set for all atoms was applied. The basis set for molybdenum was derived for this study from the def2-TZVP basis set (details and full basis set listing in Supporting Information) [30]. The basis set for fluorine was taken from our previous study on sodium hydrogen fluorides [31]. All calculations were carried out using the CRYSTAL17 program package [32]. The reciprocal space was sampled using a 5x5x5 Monkhorst-Pack-type *k*-point grid [33]. All calculations were run as spin-unrestricted (the magnetic ground state is described in the main text). For the evaluation of the Coulomb and exchange integrals (TOLINTEG), tight tolerance factors of 8, 8, 8, 8, and 16 were used. Both the atomic positions and lattice constants were fully optimized within the constraints imposed by the space group symmetry. Default optimization convergence thresholds and an extra-large integration grid (XLGRID) were applied in all calculations.

The harmonic vibrational frequencies, IR intensities, and Raman intensities were obtained through the use of the computational scheme implemented in CRYSTAL [34–37]. The Raman intensities have been calculated for a polycrystalline powder sample (total isotropic intensity in arbitrary units). The Raman final spectrum was obtained by using pseudo-Voigt peak profile (50:50 Lorenzian:Gaussian) and FWHM of 8 cm−1.When simulating the Raman spectrum, the temperature and laser wavelength were set to values corresponding to the experimental setup (T = 298.15 K, λ = 532 nm). For the IR spectrum, Lorentzian lineshape and FWHM of 8 cm−1 was used. The peak assignment was carried out by visual inspection of the normal modes (Jmol program package [19]).

In addition to the periodic calculations, molecular gas-phase calculations were carried out at the DFT-PBE0/def2-TZVP level of theory using TURBOMOLE program package [30,38,39]. Resolution of Identity (RI) approximation was used to speed up the calculations [40,41]. Intrinsic Atomic Orbitals (IAOs) and Intrinsic Bond Orbitals (IBOs) were used in the bonding analysis of the cations [42].

Appendix A. Supplementary data

Supplementary material related to this article can be found, in the online version, at doi:

Acknowledgments

Florian Kraus thanks the DFG for funding and Solvay for generous donations of F_2. Antti Karttunen thanks the Academy of Finland for funding (grant 294799) and CSC, the Finnish IT Center for Science, for computational resources. We thank Dr. Klaus Harms of the X-ray facilities at Philipps-Universität Marburg for measurement time, and Dr. Bernhard Roling for allowing us measurement time on his Raman spectrometer. Lastly, we thank Jascha Bandemehr and Lars Deubner for designing an FEP sample holder for the PPMS analysis of MoF_5 and Stefan Rudel for obtaining the single crystal data.

References

[1] R.D. Peacock, Proceedings of the Chemical Society. February 1957, Proc. Chem. Soc. (1957) 59. doi:10.1039/ps9570000033.

[2] J.R. Geichman, E.A. Smith, S.S. Trond, P.R. Ogle, Hexafluorides of Molybdenum, Tungsten, and Uranium. I. Reactions with Nitrous and Nitric Oxides, Inorg. Chem. 1 (1962) 661–665. doi:10.1021/ic50003a042.

[3] R.F. Krause, T.B. Douglas, The melting temperature, vapor density, and vapor pressure of molybdenum pentafluoride, J. Chem. Thermodyn. 9 (1977) 1149–1163. doi:10.1016/0021-9614(77)90116-1.

[4] G.H. Cady, G.B. Hargreaves, Vapour pressures of some fluorides and oxyfluorides of molybdenum, tungsten, rhenium, and osmium, J. Chem. Soc. Resumed. (1961) 1568. doi:10.1039/jr9610001568.

[5] R.T. Paine, L.B. Asprey, Reductive fluoride elimination synthesis of transition metal fluorides. Synthesis of molybdenum pentafluoride and molybdenum tetrafluoride, Inorg. Chem. 13 (1974) 1529–1531. doi:10.1021/ic50136a059.

[6] O.G. Krasnova, G.V. Girichev, A.V. Krasnov, V.D. Butskij, Ehlektronograficheskoe issledovanie stroeniya molekuly MoF5, Izv. Vysshikh Uchebnykh Zaved. Khimiya Khimicheskaya Tekhnologiya. 37(10–12) (1994) 50–56.

[7] N.I. Giricheva, O.G. Krasnova, G.V. Girichev, Simultaneous electron diffraction and mass-spectrometric study of the structure of the MoF5 molecule, J. Struct. Chem. 38 (1997) 54–61. doi:10.1007/BF02768807.

[8] R.D. Peacock, T.P. Sleight, The electronic spectra of liquid ruthenium and molybdenum pentafluorides, J. Fluor. Chem. 1 (1971) 243–245. doi:10.1016/S0022-1139(00)83218-2.

[9] N. Acquista, S. Abramowitz, Vibrational spectrum of MoF5, J. Chem. Phys. 58 (1973) 5484–5488. doi:10.1063/1.1679170.

[10] T.J. Ouellette, C.T. Ratcliffe, D.W.A. Sharp, Vibrational spectra of molybdenum and tungsten pentafluorides, J. Chem. Soc. Inorg. Phys. Theor. (1969) 2351. doi:10.1039/j19690002351.

[11] J.B. Bates, Raman spectrum of crystalline MoF5, Spectrochim. Acta Part Mol. Spectrosc. 27 (1971) 1255–1258. doi:10.1016/0584-8539(71)80077-6.

[12] Y.V. Vasil'ev, A.A. Opalovskii, K.A. Khaldoyanidi, Magnetic properties of molybdenum pentafluoride, Bull. Acad. Sci. USSR Div. Chem. Sci. 18 (1969) 231–233. doi:10.1007/BF00905525.

[13] A.M. Panich, V.K. Goncharuk, S.P. Gabuda, N.K. Moroz, Molecular and electronic structure of molybdenum pentafluoride, J. Struct. Chem. 20 (1979) 45–47. doi:10.1007/BF00746290.

[14] V.N. Ikorskii, K.A. Khaldoyanidi, Structural and phase transformations of molybdenum pentafluoride, J. Struct. Chem. 23 (1982) 302–304. doi:10.1007/BF00790778.

[15] A.J. Edwards, R.D. Peacock, R.W.H. Small, The preparation and structure of molybdenum pentafluoride, J. Chem. Soc. Resumed. (1962) 4486. doi:10.1039/jr9620004486.

[16] A.J. Edwards, G.R. Jones, Fluoride crystal structures. Part I. Tungsten oxide tetrafluoride, J. Chem. Soc. Inorg. Phys. Theor. (1968) 2074. doi:10.1039/j19680002074.

[17] B.J. Coe, S.J. Glenwright, Trans-effects in octahedral transition metal complexes, Coord. Chem. Rev. 203 (2000) 5–80. doi:10.1016/S0010-8545(99)00184-8.

[18] E.M. Shustorovich, M.A. Porai-Koshits, Y.A. Buslaev, The mutual influence of ligands in transition metal coordination compounds with multiple metal-ligand bonds, Coord. Chem. Rev. 17 (1975) 1–98. doi:10.1016/S0010-8545(00)80300-8.
[19] Jmol: an open-source Java viewer for chemical structures in 3D. http://www.jmol.org/, n.d.
[20] X-Area, STOE & Cie GmbH, Darmstadt, Germany, 2011. https://www.stoe.com/product/software-x-area/.
[21] G.M. Sheldrick, A short history of *SHELX*, Acta Crystallogr. A. 64 (2008) 112–122. doi:10.1107/S0108767307043930.
[22] G.M. Sheldrick, Crystal structure refinement with *SHELXL*, Acta Crystallogr. Sect. C Struct. Chem. 71 (2015) 3–8. doi:10.1107/S2053229614024218.
[23] H. Putz, K. Brandenburg, Diamond - Crystal and Molecular Structure Visualization, Crystal Impact, Bonn, Germany, 2015. http://www.crystalimpact.com/diamond.
[24] STOE WinXPOW, STOE & Cie GmbH, Darmstadt, Germany, 2011.
[25] V. Petříček, M. Dušek, L. Palatinus, Crystallographic Computing System JANA2006: General features, Z. Für Krist. - Cryst. Mater. 229 (2014). doi:10.1515/zkri-2014-1737.
[26] WinASPECT Plus, Jena, Germany, 2014.
[27] OPUS, Bruker Optik GmbH, Ettlingen, Germany, 2009.
[28] J.P. Perdew, K. Burke, M. Ernzerhof, Generalized Gradient Approximation Made Simple, Phys. Rev. Lett. 77 (1996) 3865–3868. doi:10.1103/PhysRevLett.77.3865.
[29] C. Adamo, V. Barone, Toward reliable density functional methods without adjustable parameters: The PBE0 model, J. Chem. Phys. 110 (1999) 6158–6170. doi:10.1063/1.478522.
[30] F. Weigend, R. Ahlrichs, Balanced basis sets of split valence, triple zeta valence and quadruple zeta valence quality for H to Rn: Design and assessment of accuracy, Phys. Chem. Chem. Phys. 7 (2005) 3297. doi:10.1039/b508541a.
[31] S.I. Ivlev, T. Soltner, A.J. Karttunen, M.J. Mühlbauer, A.J. Kornath, F. Kraus, Syntheses and Crystal Structures of Sodium Hydrogen Fluorides NaF· *n* HF (*n* = 2, 3, 4): Syntheses and Crystal Structures of Sodium Hydrogen Fluorides NaF· *n* HF (*n* = 2, 3, 4), Z. Für Anorg. Allg. Chem. 643 (2017) 1436–1443. doi:10.1002/zaac.201700228.
[32] R. Dovesi, A. Erba, R. Orlando, C.M. Zicovich-Wilson, B. Civalleri, L. Maschio, M. Rérat, S. Casassa, J. Baima, S. Salustro, B. Kirtman, Quantum-mechanical condensed matter simulations with CRYSTAL, Wiley Interdiscip. Rev. Comput. Mol. Sci. (2018) e1360. doi:10.1002/wcms.1360.
[33] H.J. Monkhorst, J.D. Pack, Special points for Brillouin-zone integrations, Phys. Rev. B. 13 (1976) 5188–5192. doi:10.1103/PhysRevB.13.5188.
[34] F. Pascale, C.M. Zicovich-Wilson, F. López Gejo, B. Civalleri, R. Orlando, R. Dovesi, The calculation of the vibrational frequencies of crystalline compounds and its implementation in the CRYSTAL code:, J. Comput. Chem. 25 (2004) 888–897. doi:10.1002/jcc.20019.
[35] C.M. Zicovich-Wilson, F. Pascale, C. Roetti, V.R. Saunders, R. Orlando, R. Dovesi, Calculation of the vibration frequencies of alpha-quartz: The effect of Hamiltonian and basis set, J. Comput. Chem. 25 (2004) 1873–1881. doi:10.1002/jcc.20120.
[36] L. Maschio, B. Kirtman, M. Rérat, R. Orlando, R. Dovesi, *Ab initio* analytical Raman intensities for periodic systems through a coupled perturbed Hartree-Fock/Kohn-Sham method in an atomic orbital basis. I. Theory, J. Chem. Phys. 139 (2013) 164101. doi:10.1063/1.4824442.
[37] L. Maschio, B. Kirtman, M. Rérat, R. Orlando, R. Dovesi, *Ab initio* analytical Raman intensities for periodic systems through a coupled perturbed Hartree-Fock/Kohn-Sham method in an

atomic orbital basis. II. Validation and comparison with experiments, J. Chem. Phys. 139 (2013) 164102. doi:10.1063/1.4824443.

[38] TURBOMOLE V7.2 2017, a development of University of Karlsruhe and Forschungszentrum Karlsruhe GmbH, 1989-2007, TURBOMOLE GmbH, since 2007; available from http://www.turbomole.com, n.d.

[39] R. Ahlrichs, M. Bär, M. Häser, H. Horn, C. Kölmel, Electronic structure calculations on workstation computers: The program system turbomole, Chem. Phys. Lett. 162 (1989) 165–169. doi:10.1016/0009-2614(89)85118-8.

[40] K. Eichkorn, O. Treutler, H. Öhm, M. Häser, R. Ahlrichs, Auxiliary basis sets to approximate Coulomb potentials, Chem. Phys. Lett. 240 (1995) 283–290. doi:10.1016/0009-2614(95)00621-A.

[41] F. Weigend, Accurate Coulomb-fitting basis sets for H to Rn, Phys. Chem. Chem. Phys. 8 (2006) 1057. doi:10.1039/b515623h.

[42] G. Knizia, Intrinsic Atomic Orbitals: An Unbiased Bridge between Quantum Theory and Chemical Concepts, J. Chem. Theory Comput. 9 (2013) 4834–4843. doi:10.1021/ct400687b.